Applied Catalysis B: Environmental 136–137 (2013) 260–268

Contents lists available at SciVerse ScienceDirect

Applied Catalysis B: Environmental

journal homepage: www.elsevier.com/locate/apcatb

High carbon-resistance Ni/$CeAlO_3$-Al_2O_3 catalyst for CH_4/CO_2 reforming

Wei Chen, Guofeng Zhao, Qingsong Xue, Li Chen, Yong Lu*

Shanghai Key Laboratory of Green Chemistry and Chemical Processes, Department of Chemistry, East China Normal University, Shanghai 200062, China

ARTICLE INFO

Article history:
Received 19 July 2012
Received in revised form 24 January 2013
Accepted 26 January 2013
Available online 8 February 2013

Keywords:
Carbon dioxide
Methane
Syngas
Nickel catalyst
Cerium
Carbon

ABSTRACT

High carbon-resistance Ni/Ce-AlO catalysts have been developed for dry reforming of methane (DRM) that is attracting growing attention for chemical recycling of CO_2 to fuels/chemicals. Cerium is definitely identified to exist in the form of $CeAlO_3$ phase after reduction at 900 °C, and so is it under running conditions. The formation of $CeAlO_3$ phase significantly enhances the catalyst carbon-resistance without decreasing the activity. Whereas the catalysts with or without $CeAlO_3$ all show good activity maintenance within 250 h testing at 800 °C using 20,000 mL h^{-1} g_{cat}^{-1}, their carbon deposition amounts exhibit significant decrease from 0.92 to 0.29 g g_{cat}^{-1} along with the increase of the $CeAlO_3$ phase. The presence of $CeAlO_3$ can inhibit growth of graphitic carbon on nickel surface while the formation of amorphous carbon is independent of the $CeAlO_3$. The $CeAlO_3$ species shows ability for decomposing CO_2 to form active surface oxygen and therefore the carbon-resistance promotion by nature is suggested to be contributed to an oxidative environment around Ni particles.

1. Introduction

Concerns about the depletion of petroleum reserves and considering the chemical recycling of CO_2 to fuels/chemicals warrant increasing attention for the catalytic process of CO_2 reforming of CH_4 (also known as dry reforming of methane, DRM, Eq. (1)), which can convert two undesirable greenhouse gases into synthesis gas [1–3].

$$CH_4 + CO_2 \rightarrow 2H_2 + 2CO, \quad \Delta H_{298} = 247\ \text{kJ mol}^{-1} \tag{1}$$

$$CH_4 + H_2O \rightarrow 3H_2 + CO, \quad \Delta H_{298} = 206\ \text{kJ mol}^{-1} \tag{2}$$

The product of the DRM process can be used as feedstock in ammonia synthesis, methanol synthesis [3,4], and especially in Fischer–Tropsch synthesis [5] due to the lower H_2/CO ratio of the synthesis gas than that of product of steam reforming of methane (SRM, Eq. (2)) [6].

Because of the high endothermicity of DRM, considerable studies have been carried out for chemical energy transmission system. This reversible endothermic reaction is driven to equilibrium state by fossil, solar energy, or nuclear energy [6,7]. By this means the DRM process store the energy in the form of synthesis gas.

As a catalytic process, supported metals of groups 8 (ruthenium), 9 (cobalt, rhodium, and iridium), and 10 (nickel, palladium, and platinum) are potential catalysts used in DRM process [8]. Although the noble metal-based catalysts are generally reported more active to reactant conversion and less sensitive to carbon deposition, their application is confined by high cost and limited availability [9–11]. From a point of view of economy, industrial practice relies on Ni-based catalysts. However, the major challenge of using Ni-based catalysts is the high thermodynamic potential to carbon deposition, which will not only induce the deactivation of catalysts, but also crush the catalysts pellets, increase the pressure drop, and even block the reactor [12]. Thus, carbon deposition has been the primary hindrance on the way to industrialization of DRM process.

For these reasons, studies on carbon deposition have been very highly regarded. Similar to the SRM, the two major carbon deposition paths, whose equilibrium constants are shown in Fig. 1, are carbon monoxide disproportionation (Eq. (3)) and methane decomposition (Eq. (4)) [1,13,14]. The former is strongly exothermic and favored at lower temperature and under higher pressure. Conversely, the latter is thermodynamically favorable at high temperature and under lower pressure.

$$2CO \rightarrow CO_2 + C, \quad \Delta H_{298} = -172\ \text{kJ mol}^{-1} \tag{3}$$

$$CH_4 \rightarrow 2H_2 + C, \quad \Delta H_{298} = 75\ \text{kJ mol}^{-1} \tag{4}$$

The mechanism of carbon formation has been well established in 1970s [14–17]. Thanks to development of the time-resolved high-resolution *in situ* transmission electron microscope (HRTEM) technique [18,19] and theoretical calculation [20,21], more details have been obtained these years. On the basis of the understanding

* Corresponding author. Tel.: +86 21 62233424; fax: +86 21 62233424.
E-mail address: ylu@chem.ecnu.edu.cn (Y. Lu).

0926-3373/$ – see front matter © 2013 Elsevier B.V. All rights reserved.
http://dx.doi.org/10.1016/j.apcatb.2013.01.044

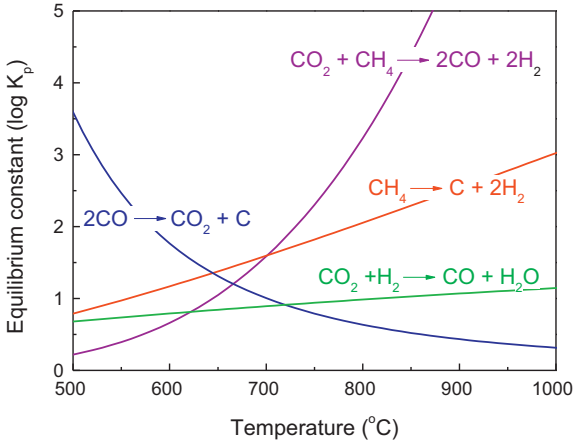

Fig. 1. Equilibrium constants of reactions (Eqs. (1)–(4)) in DRM system as a function of reaction temperature.

accumulated so far, carbon-resistance can be enhanced by using various promoters including alkaline metals [22], alkaline earth metals [23], transition metals [20,24], bio-metallic alloy [25], rare earth elements [26], or a trace of sulfur [27]. Some of these measures, regrettably, gain a better stability at the expense of catalytic activity. Studies in this field was reviewed recently by Liu et al. [28].

Cerium oxide (CeO_2) with stable fluorite structure has oxygen deficient (CeO_{2-x}, with $0 < x \leq 0.5$) in a reducing atmosphere, and this partially reduced oxide can be readily oxidized to CeO_2 by capturing oxygen in an oxidizing environment [29]. It has been reported that, owing to this peculiar oxygen capacity and structural stability, the addition of ceria could effectively improve the behavior of alumina supported catalysts used for automotive emission treatment [30] and steam reforming of gasoline [31,32]. For DRM reaction, large numbers of investigations demonstrated that ceria-containing Ni-based catalysts also exhibit a good performance in carbon-resistance [33] and other positive effects, such as improving the dispersion of the active phase [33], and preventing the transition of the γ-Al_2O_3 used as support to the low-surface-area phase α-Al_2O_3 at high temperature [34].

Despite above advances, the existing state of Ce in the working catalyst is not clear yet as well as the nature for enhanced carbon-resistance stemmed from Ce-modification over the Ni/Al_2O_3 catalyst for DRM. The goal of the present work thus is to elucidate the existing form of Ce-additives within the reaction and gain deep insight into their ability for enhanced carbon-resistance in DRM over the Al_2O_3 supported Ni catalysts. To accomplish such goal, we prepared a series of Al_2O_3-supported Ni-based (10 wt%) catalysts with CeO_2-additives in different content (0–15 wt%) *via* incipient wetness impregnation method. Long-term tests (800 °C and 20,000 mL h^{-1} g_{cat}^{-1}, $CH_4/CO_2 = 1/1$) for 250 h over as-made catalysts were carried out to reveal the effects of Ce-modification on their catalytic activity and carbon-resistance. Ce-additives were identified to exist as $CeAlO_3$ in the catalyst samples under running conditions. The presence of $CeAlO_3$ showed the ability for greatly enhancing the catalyst carbon-resistance but had no evident impact on the reactivity. To gain insight on the nature of the positive effects of $CeAlO_3$ phase, the catalyst samples were characterized systematically by the means of inductively coupled plasma atomic emission spectrometry (ICP-AES), thermogravimetric analysis (TGA), X-ray diffraction (XRD), scanning electron microscopy (SEM), transmission electron microscopy (TEM), temperature-programmed oxidation (TPO) and temperature-programmed surface reaction (TPSR) techniques. Moreover, a mechanistic model for carbon-resistance enhancement associated with the $CeAlO_3$ formation was proposed accordingly.

Table 1
Composition of studied catalysts.

Catalyst[a]	Composites (wt%)[b]			
	NiO	Ni	CeO_2	$CeAlO_3$
Fresh Ni/00Ce-AlO	10.9	–	0.0	–
Fresh Ni/05Ce-AlO	10.4	–	4.5	–
Fresh Ni/10Ce-AlO	11.2	–	9.3	–
Fresh Ni/15Ce-AlO	11.6	–	14.1	–
Used Ni/00Ce-AlO	–	9.3	–	0.0
Used Ni/05Ce-AlO	–	9.7	–	4.9
Used Ni/10Ce-AlO	–	9.9	–	10.5
Used Ni/15Ce-AlO	–	9.4	–	15.4

[a] Used catalysts were calcined at 700 °C in air to remove the carbon deposition completely and washed in ultrasonic cleaner, prior to ICP-AES sample preparation.
[b] For all the samples used for ICP-AES determination, Ni and Ce are in form of NiO and CeO_2, respectively. However, according to the XRD results, Ni and Ce in working condition are in the form of metallic Ni and $CeAlO_3$ which will be discussed later. So the composites were calculated stoichiometrically by balancing O to the form of Ni and $CeAlO_3$ with the assumption that CeO_2 were completely reduced to $CeAlO_3$ (see S-1 in Supporting Information).

2. Experimental

2.1. Catalyst preparation

Ce-modified Al_2O_3 supports with CeO_2 loadings of 5 wt%, 10 wt% and 15 wt% were prepared by incipient wetness impregnation of γ-Al_2O_3 (Alfa Aesar, surface area = 247 m^2 g^{-1}; crushed and collected the particle of 0.15–0.18 mm), using an aqueous solution of $Ce(NO_3)_3{\cdot}6H_2O$ (Sinopharm Chemical Reagent Co., Ltd.) as precursor. Then the products were dried at 100 °C overnight and calcined at 450 °C in static air for 2 h with a ramp of 2 °C min^{-1}. To load 10 wt% Ni as active phase, the support (with or without CeO_2-promotion) was incipiently impregnated with aqueous solution of $Ni(NO_3)_2{\cdot}6H_2O$ (Sinopharm Chemical Reagent Co., Ltd.). The as-made products were dried overnight and calcined at 500 °C in air for 5 h with a ramp of 2 °C min^{-1}. The final products with 10 wt% Ni as active phase and with 0 wt%, 5 wt%, 10 wt% and 15 wt% CeO_2 as modifier were denoted as Ni/00Ce-AlO, Ni/05Ce-AlO, Ni/10Ce-AlO and Ni/15Ce-AlO, respectively.

2.2. Catalyst characterization

The exact composition of the catalysts was determined by using a Thermo Scientific iCAP 6300 inductively coupled plasma atomic emission spectrometry (ICP-AES). The results are listed in Table 1.

X-ray diffraction (XRD) patterns were obtained with a Rigaku Ultra IV diffractometer using Cu Kα radiation at 35 kV and 25 mA in the 2θ scanning range of 20–80° and scanning rate of 10° min^{-1}. Working-line determined by 5 points was employed to determine the content of graphitic carbon.

Thermogravimetric analysis (TGA) of the used catalysts was carried out on a Mettler-Toledo TG-SDTA-851 analyzer to determine the total amount of carbon on used catalysts.

The scanning electron microscopy (SEM) images and back-scattering electron (BE) images were obtained on a Hitachi S-4800 microscopy. Each BE image was captured at the same area as the corresponding SEM image. The transmission electron microscopy (TEM) images were obtained on a JEOL-JEM-2010 microscopy.

Experiments on temperature-programmed oxidation (TPO) and temperature-programmed surface reaction (TPSR) were performed on a Quantachrome CHEMBET-3000 instrument equipped with a thermal conductivity detector (TCD). The products were also analyzed by an on-line mass spectrometer (AMETEK ProLine Mass Spectrometer). Typically, 50 mg of catalyst was loaded into a U-shaped quartz tube with quartz wool at both sides. For O_2-TPO and sequential CO_2-TPO/O_2-TPO, samples were pre-treated in He flow

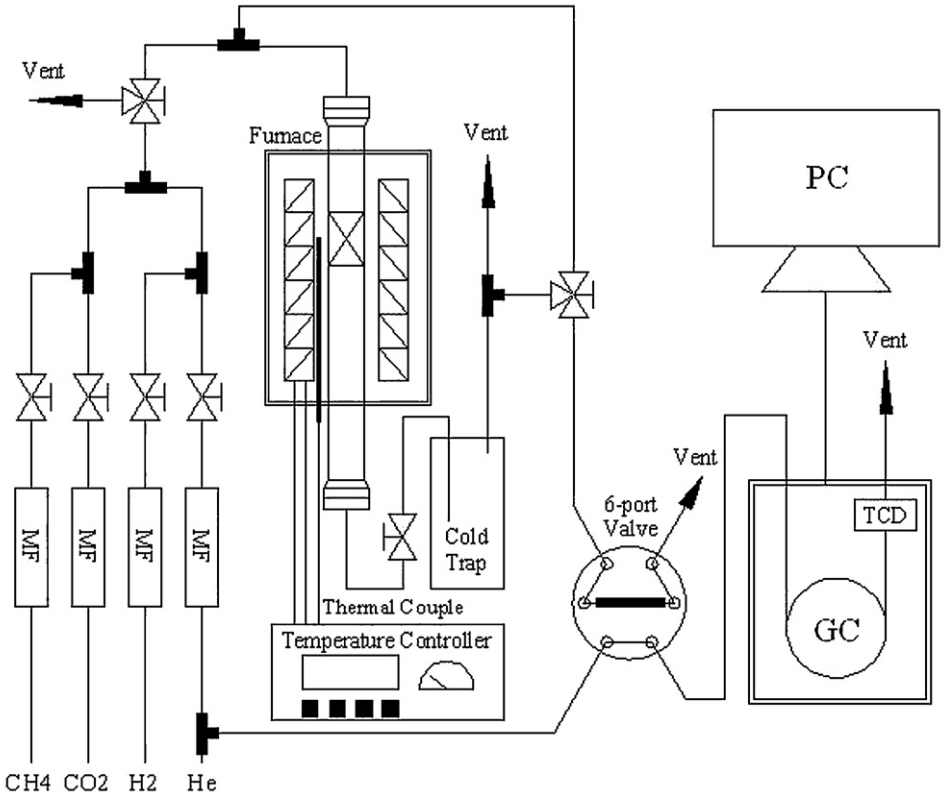

Fig. 2. Schematic diagram of the apparatus for catalysts evaluation.

at 300 °C for 1 h and then cooled down to 200 °C. After that, the gas mixture (5% O_2 in He or 10% CO_2 in He) was fed to the tube with a total flux of 50 ml min^{-1} and the sample was then heated up to 800 °C with the ramp of 10 °C min^{-1}. For CH_4-TPSR or CO_2-TPSR experiments, the samples were reduced *ex situ* with pure H_2 at 900 °C for 1 h in advance. After *ex situ* reduction, the samples were charged and reduced *in situ* with 5% H_2 in Ar at 600 °C for 1 h followed by cooling down to 200 °C. Then, the reactant gas (5% CH_4 in He or 10% CO_2 in He) was fed with a total flux of 50 ml min^{-1} into the reactor bed where the samples were heated up to 900 °C with a ramp of 10 °C min^{-1} and kept at 900 °C for 20 min. In sequential CO_2-TPO/O_2-TPO experiments, as soon as the last step ended, the sample was cooled down quickly in He flow by exposing the reactor into the ambient environment.

2.3. Long-term tests

Long-term tests of the catalysts were conducted in a quartz tube reactor with inner diameter of 16 mm. The schematic diagram of the apparatus was drawn in Fig. 2. For each run, 300 mg of sample was loaded without any dilution and reduced *in situ* with a pure H_2 (99.999%) flow (30 mL min^{-1}) at 900 °C (heating rate 2 °C min^{-1}) for 1 h flowed by cooling down to desired temperature in He flow. Then, an equimolar feed gas of CH_4 (99.99%) and CO_2 (99.995%) with total flux of 100 mL min^{-1} (GHSV = 20,000 mL h^{-1} g_{cat}^{-1}) was introduced into the catalytic bed. Tests were carried out at 800 °C

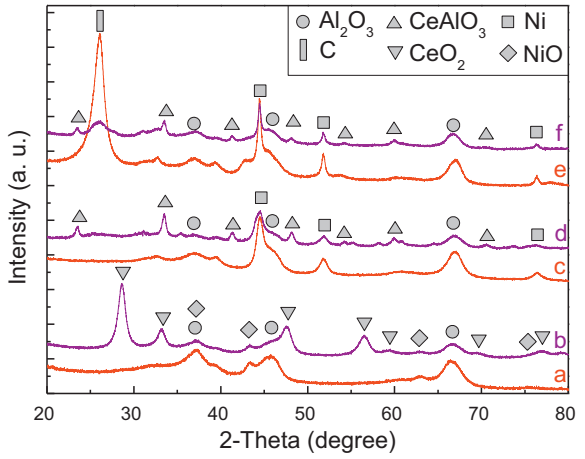

Fig. 3. XRD patterns of the catalysts in three stages: (a) fresh Ni/00Ce-AlO, (b) fresh Ni/15Ce-AlO, (c) reduced Ni/00Ce-AlO, (d) reduced Ni/15Ce-AlO, (e) used Ni/00Ce-AlO, and (f) used Ni/15Ce-AlO.

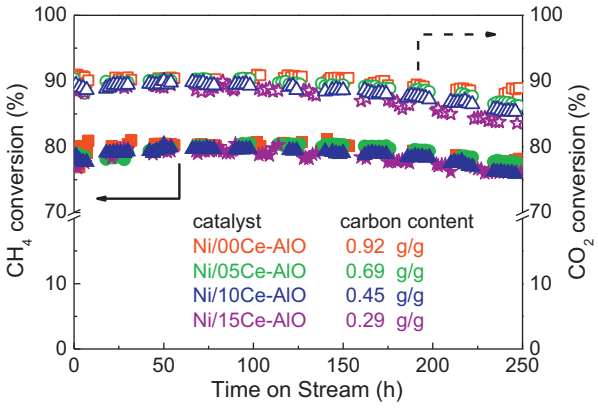

Fig. 4. Activity performance and carbon content of the catalysts in 250 h long-term tests. Reaction conditions: 800 °C, GHSV = 20,000 mL min^{-1} g^{-1}, atmospheric pressure. Square: Ni/00Ce-AlO; circle: Ni/05Ce-AlO; triangle: Ni/10Ce-AlO; star: Ni/15Ce-AlO.

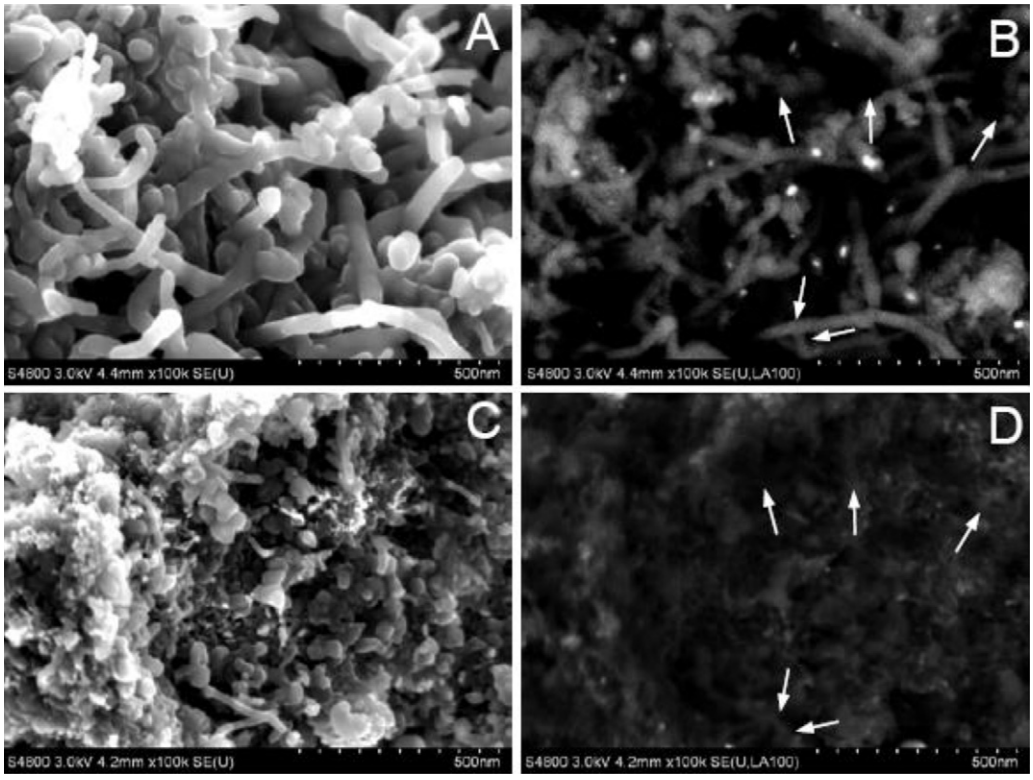

Fig. 5. SEM ((A) Ni/00Ce-AlO and (C) Ni/15Ce-AlO) and BE ((B) Ni/00Ce-AlO and (D) Ni/15Ce-AlO) images of the catalysts after 250 h DRM tests at 800 °C.

under atmospheric pressure. The reactants and products were analyzed by HP 6850 GC equipped with TCD connected to Plot Q and MS 5A parallel capillary column (DIKMA).

3. Results and discussion

3.1. XRD phases of catalysts

The bulk phases of the representative Ni/15Ce-AlO catalysts as well as the catalyst without Ce-modification (Ni/00Ce-AlO) in three stages (fresh, reduced and used) were determined by XRD as presented in Fig. 3. For the fresh catalysts calcined at 500 °C for 5 h, Ce is observed evidently in the form of CeO_2 while no distinct peaks corresponding to NiO can be identified, indicating the high dispersion of NiO due to the well-known strong interaction between NiO and Al_2O_3 [35]. After reduction at 900 °C for 1 h in H_2, NiO was reduced to metallic nickel with the size of 8.2–9.7 nm as estimated by Scherrer's equation. Along with the NiO reduction, the CeO_2 phase disappeared while a new phase of $CeAlO_3$ was formed [36]. Here we proposed that, after reduction at 900 °C, CeO_2 was reduced to $CeAlO_3$ completely [37,38] (see S-1 including Figs. S1 to S5 in Supporting Information for more details). After undergoing DRM at 800 °C even for 250 h, except the new graphitic carbon peak at 26° (it will be discussed in detail posteriorly), XRD patterns of the used catalysts remained almost unchanged in comparison with the reduced one. Notably, bulk-phase $CeAlO_3$ was not formed in the Ni/15Ce-AlO pre-reduced in H_2 at 800 °C for 1 h (Fig. S4a in Supporting Information). However, when this catalyst sample underwent DRM reaction at 800 °C for 18 h, XRD patterns of $CeAlO_3$ phase (Fig. S4b in Supporting Information) was observed clearly to be compatible to the sample pre-reduced at 900 °C (Fig. 3d). It is thus believed that cerium is presented in the form of $CeAlO_3$ phase under the running conditions.

However, we wonder whether the $CeAlO_3$ phase is crucial for the carbon-resistance improvement for the Ce-modified Ni/Al_2O_3 catalysts or not. If so, it is particularly desirable to clarify how the $CeAlO_3$ phase enhanced the carbon-resistance of the Ni/Ce-AlO catalysts.

3.2. Carbon-resistance

Long-term DRM tests were carried out over the catalysts with varied $CeAlO_3$ contents for carbon deposit measurement at 800 °C using GHSV of 20,000 mL h^{-1} $g_{cat}{}^{-1}$. Fig. 4 shows the conversion and the amount of carbon deposit within 250 h tests. As we can see, all the catalysts with $CeAlO_3$ content ranged from 0 to 15 wt% exhibited compatible catalytic conversion and reactivity maintenance throughout the 250 h tests. It should be noted that the conversion of CO_2 is slightly higher than that of CH_4 throughout the test. It is likely because of a certain extent of the reverse water gas shift (RWGS) reaction [1–3], which converts additional CO_2. This inference can also be proved by the fact that the water condensed in cold trap was at the average rate of 0.15 g h^{-1}.

Unlike the conversion maintenance, the amount of carbon on each catalyst changed evidently, being reduced from 0.92 to 0.29 g $g_{cat}{}^{-1}$ along with the increase of $CeAlO_3$ content from 0 to 15 wt%. It seems undoubtedly that the Ce existed in form of $CeAlO_3$ has the ability of suppressing the carbon deposition in DRM over the Ni/Ce-AlO catalysts.

A rough calculation indicated that the CO formation is at least three orders of magnitude faster than the carbon deposition within such long-term test. The carbon deposition rate thus showed negligible impact on apparent activity. Note that much higher $CeAlO_3$ content (*e.g.*, ≥20 wt%) would visibly deteriorate the catalytic activity, *e.g.*, methane conversion at 800 °C: 80% over Ni/00Ce-AlO, 78% over Ni/15Ce-AlO, and only 75% over Ni/20Ce-AlO (20 wt% $CeAlO_3$ as modifier). The catalysts with $CeAlO_3$ higher than 15 wt% were thus not employed to undergo long-term tests for carbon deposit measurement.

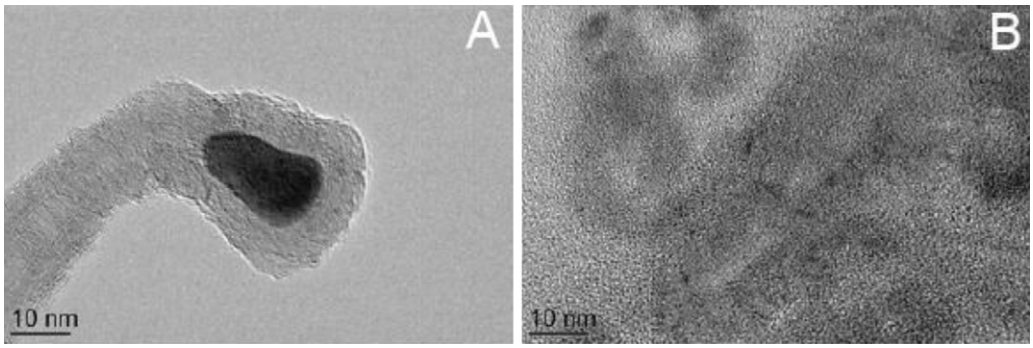

Fig. 6. TEM images of the Ni/00Ce-AlO (A) and Ni/15Ce-AlO (B) after 250 h DRM tests at 800 °C.

3.3. Structure of carbon deposits

3.3.1. SEM and TEM

Fig. 5 shows the SEM and BE images of the Ni/00Ce-AlO and Ni/15Ce-AlO catalysts after 250 h tests at 800 °C. It is not surprising that a large quantity of filamentous carbon is observed on Ni/00Ce-AlO catalyst (Fig. 5A). Meanwhile, many bright spots in the BE images of Ni/00Ce-AlO catalyst (Fig. 5B) could be observed, showing that most nickel particles were observed at the head of filaments. According to Baker's study [15], this kind of filamentous carbon is generally produced from the metal-catalyzed methane. In contrast, the filaments rooting in Ni/15Ce-AlO catalyst surface are much less, shorter and thinner than those on the Ni/00Ce-AlO catalyst (Fig. 5C), and few of encapsulated nickel particles can be observed in the BE images (Fig. 5D). In addition, some moss-like carbon that has been described by Matsukata [39] was clearly observed on the used Ni/15Ce-AlO catalyst (Fig. 5C).

TEM analyses were then carried out for more details in carbon deposited on such used catalysts with the images as shown in Fig. 6. For the Ni/00Ce-AlO catalyst (Fig. 6A), Ni particles were observed to be encapsulated in the tip of filamentous carbon with clear graphitic basal planes. This structure is well consistent with the growth mechanism suggested by Baker and Rostrup-Nielsen [15–18], *i.e.*, the filamentous carbons grow catalytically at one side of the nickel particle and separate out as carbon filament on the other side of the nickel particle. For the Ni/15Ce-AlO (Fig. 6B), though distorted graphitic basal planes can be identified, no particular appearance of carbon whiskers can be clearly figured out. This kind of carbon with disordered structure can be assigned to moss-like amorphous carbon in Fig. 5C, and cannot be detected apparently by XRD.

3.3.2. TPO

Direct O_2-TPO and sequential CO_2-TPO/O_2-TPO were performed to study the reactivity of the carbon deposits formed on the used catalyst samples, with the results as shown in Fig. 7. Direct O_2-TPO results as shown in Fig. 7A indicated that all samples provided an asymmetric peak, likely due to the peak overlap of both filamentous carbon and amorphous carbon. Regardless of the poor revolution of the O_2-TPO for distinguishing filamentous and amorphous carbons, the O_2-TPO peak area that represents the carbon content gradually decreased along with the $CeAlO_3$ content in the catalyst (Fig. 7A), being in good agreement with carbon reduction indication with various $CeAlO_3$ content as shown in Fig. 4.

Fig. 7B shows the CO_2-TPO profiles of the catalyst samples same as employed in Fig. 7A, indicating that CO_2-oxidizable carbon could be clearly detected on the used catalyst samples except Ni/15Ce-AlO within the testing temperature range. Note that the amount of such CO_2-oxidizable carbon was correspondingly reduced along with the $CeAlO_3$ content. Fig. 7C shows the subsequent O_2-TPO profiles after the above CO_2-TPO experiments. Unlike the asymmetric peaks in Fig. 7A, nearly symmetrical peaks were presented while showing almost equivalent peak area.

Matsukata and Yang reported that the filamentous carbon with graphitic structure could be gasified by CO_2, and the amorphous moss-like carbon, oppositely, could not be removed readily by oxidation with CO_2 [39–41]. Takenaka and Nagaoka independently reported that the carbon on metal can be removed by CO_2, but carbon without metal cannot be removed below 800 °C [42–44]. Combining above literature information with our observations from SEM and TEM (Figs. 5 and 6), we believed that the CO_2-oxidizable carbon in Fig. 7B is assignable to the filamentous carbon and the Ni particles on the filamentous carbon show ability to catalyze the reaction of such carbon with CO_2. The carbon in Fig. 7C thus is assignable to the amorphous carbon with lower-order structure deposited on the support, which cannot be oxidized by CO_2 during CO_2-TPO. Nevertheless, it is clear from Fig. 7C that the maximum O_2-TPO peak temperature of the amorphous carbon showed a gradual reduction from ~710 °C to ~550 °C along with the increase of $CeAlO_3$ from 0% up to 15%. It can be rationally inferred that the presence of $CeAlO_3$ shows the ability for O_2 activation to form CeO_2 species (Fig. S5 in Supporting Information) thereby promoting the low-temperature oxidation of the amorphous carbon.

3.4. $CeAlO_3$ suppressing filamentous carbon growth

Fig. 8 shows the XRD patterns of the used catalysts same as in Figs. 5 and 6. We here focused on the notable peaks at 26° which are attributed to filamentous carbon with graphitic structure [45,46]. Since the amorphous carbon will not be detected by XRD,

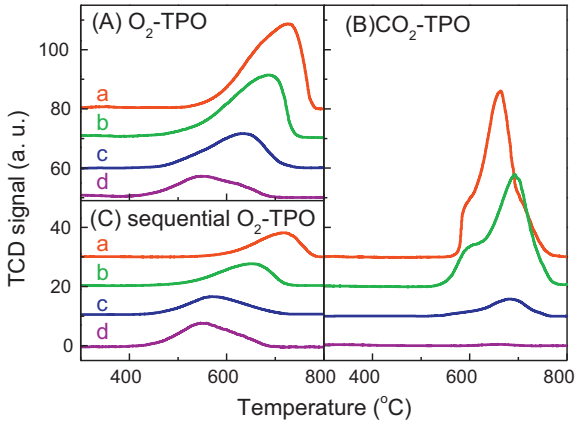

Fig. 7. O_2-TPO (A) and sequential CO_2-TPO/O_2-TPO (B and C) profiles of the catalysts after 250 h DRM tests at 800 °C. (a) Ni/00Ce-AlO, (b) Ni/05Ce-AlO, (c) Ni/10Ce-AlO and (d) Ni/15Ce-AlO.

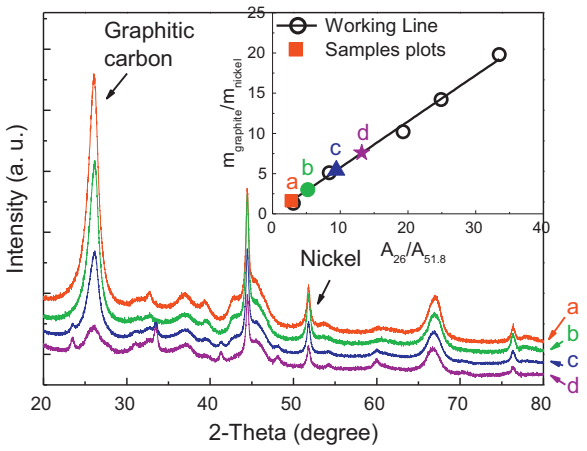

Fig. 8. XRD patterns of the catalysts after 250 h DRM tests at 800 °C. The XRD working-line is shown as inset. (a) Ni/00Ce-AlO, (b) Ni/05Ce-AlO, (c) Ni/10Ce-AlO and (d) Ni/15Ce-AlO.

content of filamentous carbon in the used catalysts can be quantitatively determined, using the working curve method on the basis of peak area ratio of filamentous carbon at 26° to nickel. Here, the Ni (2 0 0) diffraction peak at 51.8° was chosen as standard to avoid interference from Al_2O_3 support. By characterizing five standard samples containing known concentrations of the graphite in fine nickel powder, the working curve of $A_{26}/A_{51.8}$ (XRD peak area ratio of graphite at 26° to nickel at 51.8°) was plotted against $m_{graphic}/m_{Ni}$ (weight ratio of graphitic carbon to nickel) and placed in Fig. 8 as an inset. With the aid of working curve method, the content of filamentous carbon in the used catalyst samples can be determined, and in turn the content of amorphous carbon can be calculated easily by subtracting the filamentous carbon fraction from total carbon content.

Fig. 9 shows the content evolution behavior of filamentous and amorphous carbons against the $CeAlO_3$ content in the used catalyst samples. Along with the increase of $CeAlO_3$ from 0 to 15 wt%, interestingly, the graphitic filamentous carbon (estimated by XRD) in the used catalysts was gradually decreased from 0.76 to 0.16 g g_{cat}^{-1} while the content of amorphous carbon seemed independent of $CeAlO_3$ and always remained at ~0.15 g g_{cat}^{-1}. As well known, the filamentous carbon with graphitic structure is formed by metal-catalyzed methane [14–21]; the moss-like amorphous carbon is mostly produced through thermal cracking of methane (see S-2 including Figs. S6 and S7 in Supporting Information) [13]. It is thus rational for us to infer from the above results that, the Ce-additive existed in the form of $CeAlO_3$ phase shows the ability to significantly suppress the filamentous carbon formation route by metal-catalyzed methane but not the amorphous carbon formation *via* the thermal cracking of methane.

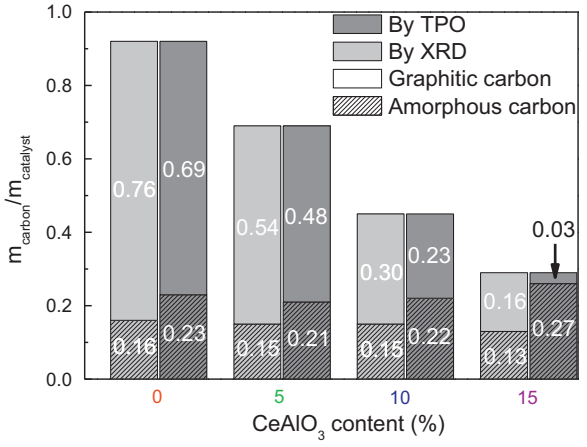

Fig. 9. Contents of graphitic carbon (blank) and amorphous carbon (shadow) on used catalysts with different $CeAlO_3$ content estimated by two measures: XRD (dark gray) and TPO (light gray).

Moreover, the fractions of amorphous carbon and filamentous carbon on the used catalyst samples could also be estimated from the peak area data in Fig. 7A and C. For example, peak area of the profile (a) in Fig. 7A represented the total carbon amount on the used Ni/00Ce-AlO catalyst and that of the profile (a) in Fig. 7C is the amount of amorphous carbon. Thus, the peak area ratio of the latter to that of the former is estimated to be the fraction of amorphous carbon on the used Ni/00Ce-AlO catalyst. The carbon distribution fractions are also displayed in Fig. 9. Whereas the results from TPO experiments were not entirely identical to the values derived from XRD analyses, the amount of filamentous carbon from TPO experiments similarly shows visible reduction along with increase of $CeAlO_3$ content while the amorphous carbon amount almost remains unchanged yet. The $CeAlO_3$ exhibits the ability to strongly suppress the growth of filamentous carbon but become helpless to attenuate the formation of amorphous carbon.

Over the catalyst with less $CeAlO_3$, more Ni particles will be raised up and pushed forward by the growing carbon whisker [18]. By this way, the Ni particles are still available for reaction, and did not impact the reaction conversion significantly [12]. In contrast, the amorphous carbon accumulating on the catalyst surface will shield the Ni particles thereby decreasing the reaction conversion. So, it is the possible reason why the catalyst with more $CeAlO_3$ experienced more loss of conversion throughout the 250 h test.

3.5. *In-depth understanding of $CeAlO_3$ for carbon resistance promotion*

3.5.1. *Nickel particle size and dispersion*

The positive effect of $CeAlO_3$ on Ni dispersion was observed only at high temperature of 1100 °C which was not employed in real operation. TEM images (Fig. S8) of samples reduced at different temperatures gave direct observation. As shown, the reduction of Ni particle size due to the Ce addition, or the effect of $CeAlO_3$ on Ni dispersion, became evident only when reduction temperature was as high as 1100 °C. In XRD patterns of the reduced samples (Fig. S9), the peaks corresponding to metallic nickel all became sharper with increasing the reduction temperature for catalysts with and without Ce additives. The average particle size (estimated by Scherrer's equation) of 10Ni/AlO and 10Ni/15Ce-AlO as function of reduction temperature was plotted in the inset of Fig. S9. Being consistent with the TEM observation, $CeAlO_3$ was clearly found to be able to suppress the sintering of Ni particle only at extremely high reduction temperature of 1100 °C. In addition, it was also found that the $CeAlO_3$ can effectively prevent the transition of the γ-Al_2O_3 support to the low-surface-area phase α-Al_2O_3 at high temperature.

Although it was reported that the carbon deposition was significantly suppressed on the Ni particles smaller than 5 nm [20], the Ni particle size in both catalysts with and without Ce additives always remained at around 10 nm at or below reduction temperature of 900 °C (inset of Fig. S9). It is thus reasonable for us to rule out the contribution of Ni dispersion on the carbon resistance promotion.

3.5.2. *Sequential CH_4-TPSR/CO_2-TPO/O_2-TPO*

Carbon deposition, although, originates from two reaction, *i.e.*, carbon monoxide disproportionation (Eq. (3)) and methane decomposition (Eq. (4)), most researchers proposed that the latter is the main cause [11,47–49]. We thus wonder whether the $CeAlO_3$ affects the CH_4 decomposition thereby promoting the catalyst carbon

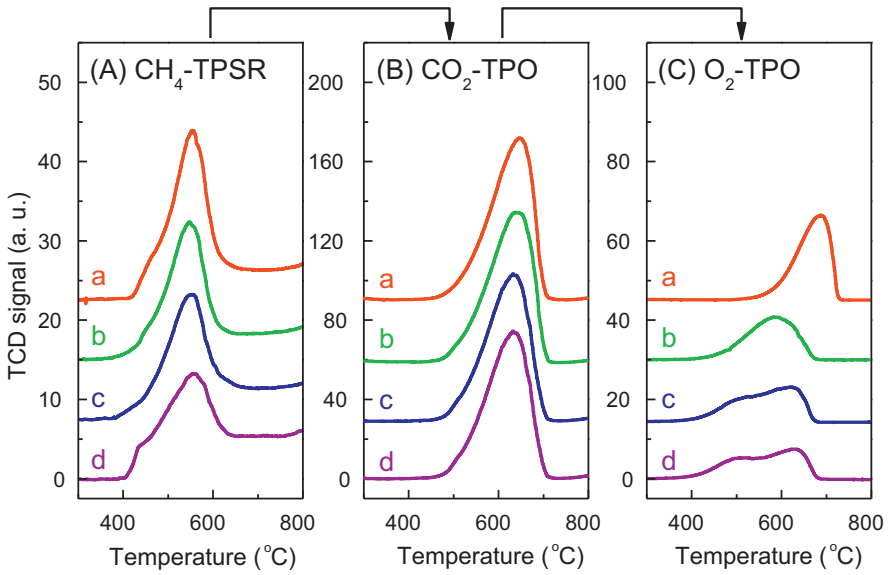

Fig. 10. Sequential CH_4-TPSR/CO_2-TPO/O_2-TPO profiles of the catalysts: (a) Ni/00Ce-AlO, (b) Ni/05Ce-AlO, (c) Ni/10Ce-AlO and (d) Ni/15Ce-AlO.

resistance. To answer this question, sequential CH_4-TPSR/CO_2-TPO/O_2-TPO experiments were performed, with the results as shown in Fig. 10. Clearly, all the catalyst samples, with or without $CeAlO_3$, presented quite similar CH_4-TPSR profiles. This indicated that the presence of $CeAlO_3$ almost did not affect the CH_4 decomposition on the nickel particles. Subsequent CO_2-TPO/O_2-TPO results showed that compatible amount of carbon was formed on all the catalyst samples after CH_4-TPSR, further indicating the methane decomposition independent of $CeAlO_3$. Notably, all the catalyst samples provided almost the same profiles, with respect to the peak area and maximum peak temperature, in the subsequent CO_2-TPO experiments. This indicated that both the reactivity with CO_2 and the amount of such carbon formed from Ni-catalyzed methane were independent of $CeAlO_3$.

It is rational for us to infer, from such independence of $CeAlO_3$ with Ni-catalyzed-methane carbon formation and sequential removal by CO_2 oxidization (Fig. 10), that the filamentous carbon in the DRM was suppressed by the $CeAlO_3$ most likely through chemically blocking its growth rather than post CO_2-oxidation removal. If not so, compatible amount of filamentous carbon should be formed on all four catalyst samples after 250 DRM tests because of their identical ability for catalytic decomposition of methane (Fig. 10A) together with their comparable activity for DRM reaction (Fig. 4).

3.5.3. CO_2-TPSR

Fig. 11 shows the CO_2-TPSR profiles on the pre-reduced catalyst samples with and without $CeAlO_3$. As we can see, all catalyst samples provided a symmetric broad CO_2 consumption peak. The Ni/00Ce-AlO catalyst delivered a weak peak with maximum temperature of 810 °C, being due to the oxidation of metallic nickel. Notably, along with the increase of $CeAlO_3$ content, the peak area was gradually increased while the maximum peak temperature showed a shift to low temperature. For example, the peak area for the Ni/15Ce-AlO catalyst was estimated to be 8 times larger than that for the Ni/00Ce-AlO catalyst, while its maximum peak temperature was 130 °C lower than that (810 °C) for the Ni/00Ce-AlO catalyst. We believe that the significant enhancement of CO_2 consumption was contributed to the reaction of $CeAlO_3$ with CO_2 to a kind of surface active oxygen [50], further solidly evidenced by the mass spectrum for CO formation synchronously accompanied by CO_2 consumption. Moreover, the nickel could catalyze the dissociation of CO_2 on the $CeAlO_3$ thereby leading to visible reduction of the peak temperature. Indeed, $CeAlO_3$ in the 15Ce-AlO support just could be oxidized by CO_2 at above 600 °C (maximum peak temperature: >900 °C), with a large peak area. Quasi-quantitative estimation showed that the total CO_2 consumption over Ni/00Ce-AlO catalyst and 15Ce-AlO support was approximately equal to that over Ni/15Ce-AlO catalyst. Fig. 12 shows the XRD patterns of Ni/15Ce-AlO catalyst samples before and after CO_2-TPSR. It is not surprising that phase transformation from $CeAlO_3$ and Ni to CeO_2 and NiO really occurred because of the deep oxidation after undergoing CO_2-TPSR. In other words, the $CeAlO_3$ with the ability of capturing the CO_2 to form active surface oxygen can be oxidized to CeO_2 due to its reducibility.

3.5.4. *Chemistry understanding of $CeAlO_3$ for carbon resistance promotion*

On the basis of foregoing results, we believed that the $CeAlO_3$ shows the ability to kinetically suppress the filamentous carbon formation in the DRM reaction by chemically blocking its growth rather than post CO_2-oxidation removal, as described by Scheme 1.

It is generally accepted that the CH_4 molecules were decomposed on nickel surface to reactive species CH_x (x=0–3) [48],

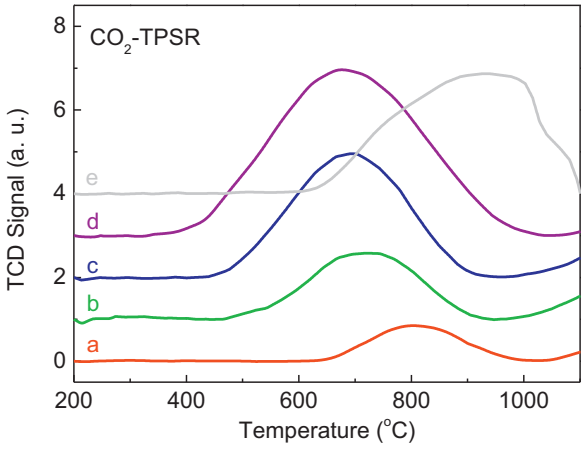

Fig. 11. CO_2-TPSR profiles of the catalysts: (a) Ni/00Ce-AlO, (b) Ni/05Ce-AlO, (c) Ni/10Ce-AlO, (d) Ni/15Ce-AlO and (e) 15Ce-AlO support.

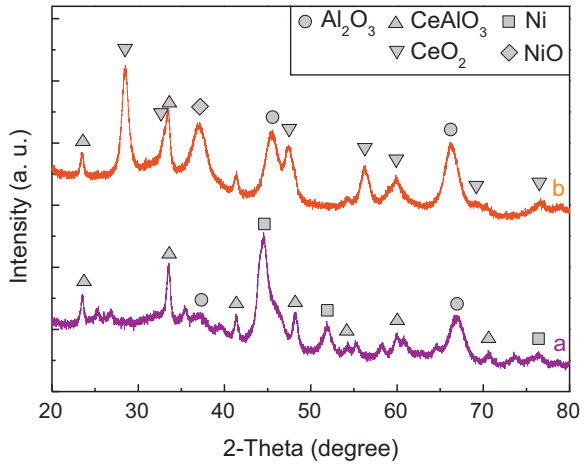

Fig. 12. XRD patterns of the 10Ni/15Ce-AlO catalyst before (a) and after (b) CO_2-TPSR.

while the CO_2 molecules were chemisorbed and dissociated on metal surface [1], or form carbonate-like species on support surface [48]. The gasification of adsorbed carbon from CH_4 fragments is thought to process on nickel surface as well as at the boundary of nickel–support. Nagaoka suggested that the reactivity on metal–support boundary is higher than that on metal surface [44]. Some isolated carbon atoms, which were not gasified immediately, will diffuse either on nickel surface or through the bulk to reach the nickel–support interface [21,47,51]. The active oxygen [50] or carbonate from CO_2 [33,52] on support will oxidize the carbon atoms to form CO. However, if the carbon atom at nickel–support interface has not been gasified immediately, the nucleation and growth of graphene layers will occur, assisted by a dynamic formation and restructuring of mono-atomic step edges at nickel–support boundary, which are considered more active sites than terrace sites in carbon nucleation [20,53]. The consecutive formation of more graphene sheets elongate nickel particle and orient their basal plane (0 0 2) parallel to the nickel surface. The nickel particles, finally, will be raised up and pushed forward by the growing carbon filaments [18] (as shown in Fig. 6A and Scheme 1). Once the nickel particles are separated from the catalysts, the filamentous carbon with graphitic structure will not be removed by CO_2 any more in DRM reaction conditions [42,43].

Most notably, $CeAlO_3$ with the ability of capturing the CO_2 to form active surface oxygen can be oxidized to CeO_2 due to its reducibility. Furthermore, it is reported that the surface basicity of CeO_2 is definitely higher than that of Al_2O_3 and the interaction of CeO_2 and CO_2 would yield considerable carbonate species which can react with CH_x species [33,52]. Two overall reactions can be rationally proposed as shown in Eqs. (5) and (6).

$$2CeAlO_3 + CO_2 \rightarrow Al_2O_3 + 2CeO_2 + CO \quad (5)$$

$$Al_2O_3 + 2CeO_2 + CH_x \rightarrow CO + 2CeAlO_3 + (x/2)H_2 \quad (6)$$

The gasification of surface carbon at nickel–support boundary is readily promoted due to the combination of CO_2 activation and Ce^{3+}/Ce^{4+} cycling, thus decreasing the possibility of graphene layer formation thereby kinetically suppressing the carbon deposition to a great extent. That is reasonable to say, the carbon formation on Ni/Al_2O_3 was suppressed because of the oxidative environment around Ni particles on $CeAlO_3$-promoted Al_2O_3 support (Scheme 1). On the other hand, the thermal cracking of hydrocarbon is a homogenous process which will not be affected significantly by the properties of catalyst. Actually, as shown in Fig. 9, the contents of amorphous carbon on the catalyst samples after 250 h DRM tests are quite similar with each other, but the graphitic carbons are highly suppressed.

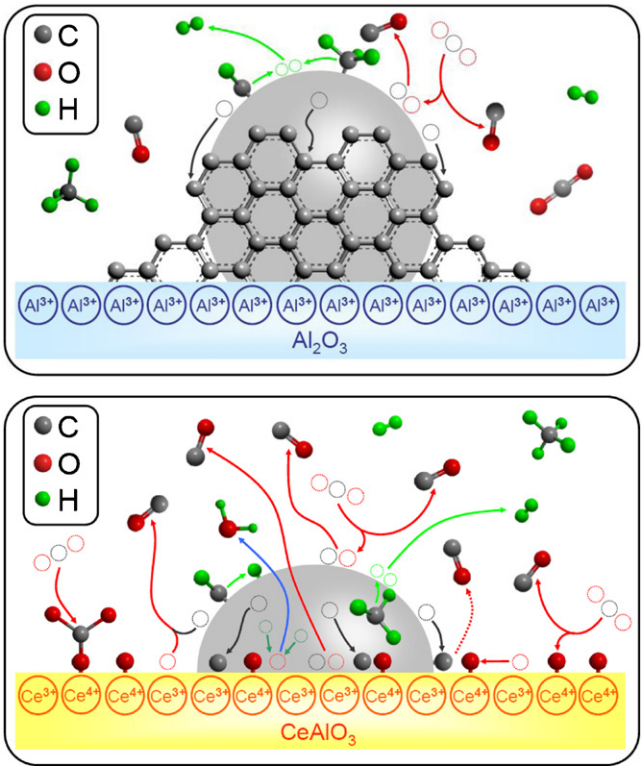

Scheme 1. Schematic representation of reaction and carbon deposition over Ni/Al_2O_3 (upper) and Ni/Ce-AlO (down) catalysts.

4. Conclusions

Our results establish that the carbon-resistance of a Ni/AlO catalyst with Ni-loading of 10 wt% for DRM can be significantly improved by Ce-modification. The $CeAlO_3$ phase formed in pre-reduction stage can remain unchanged in DRM reaction. It is found that the $CeAlO_3$ phase exhibits the ability to suppress the carbon deposition without deteriorating the activity, mainly as a function of $CeAlO_3$ content in the catalysts. The most promising catalyst is the one with $CeAlO_3$ loading of 15 wt%, on which the carbon deposit is only 0.29 g g_{cat}^{-1} after 250 h testing at 800 °C using 20,000 mL h^{-1} g_{cat}^{-1}, less than a third that (0.92 g g_{cat}^{-1}) on the Ni/Al_2O_3 catalyst. We find that the $CeAlO_3$ possesses the ability to inhibit the growth of filamentous carbon on nickel surface while the formation of amorphous carbon *via* thermal cracking of methane is independent of the $CeAlO_3$. By nature, the $CeAlO_3$ is active for catalytically decomposing CO_2 to form active surface oxygen. As a result, oxidative environment around Ni particles is suggested to be formed and therefore the carbon atom at nickel–support interface can be gasified immediately before the nucleation and growth of graphene layers.

Acknowledgements

This work was funded by the NSF of China (21273075, 21076083, 20973063), the "973 program" (2011CB201403) from the MOST of China, and the Specialized Research Fund for the Doctoral Program of Higher Education (20090076110006).

Appendix A. Supplementary data

Supplementary data associated with this article can be found, in the online version, at http://dx.doi.org/10.1016/j.apcatb.2013.01.044.

References

[1] M.C. Bradford, M.A. Vannice, Catalysis Reviews: Science and Engineering 41 (1999) 1–42.
[2] M.S. Fan, A.Z. Abdullah, S. Bhatia, ChemCatChem 148 (2009) 191–205.
[3] W. Chen, W.Q. Sheng, G.F. Zhao, F.H. Cao, Q.S. Xue, L. Chen, Y. Lu, RSC Advances 2 (2012) 3651–3653.
[4] J.R.H. Ross, A.N.J. van Keulen, M.E.S. Hegarty, K. Seshan, Catalysis Today 30 (1996) 193–199.
[5] V.F. Fischer, H. Tropsch, Brennstoff Chemie 3 (1928) 39–46.
[6] S.B. Wang, G.Q.M. Lu, Energy & Fuels 10 (1996) 896–904.
[7] A. Steinfeld, R. Palumbo, Solar thermochemical process technology, in: R.A. Meyers (Ed.), Encyclopedia of Physical Science & Technology, vol. 15, Academic Press, Inc., San Diego, 2001, pp. 237–256.
[8] G. Jones, J.G. Jakobsen, S.S. Shim, J. Kleisa, M.P. Andersson, J. Rossmeisl, F. Abild-Pedersen, T. Bligaard, S. Helveg, B. Hinnemann, J.R. Rostrup-Nielsen, I. Chorkendorff, J. Sehested, J.K. Nøskov, Journal of Catalysis 259 (2008) 147–160.
[9] A.T. Ashcroft, A.K. Cheetham, M.L.H. Green, P.D.F. Vernon, Nature 352 (1991) 225–226.
[10] J.H. Bitter, K. Seshan, J.A. Lercher, Journal of Catalysis 171 (1997) 279–286.
[11] J.R. Rostrup-Nielsen, J.H.B. Hansen, Journal of Catalysis 144 (1993) 38–49.
[12] J. Sehested, Catalysis Today 111 (2006) 103–110.
[13] C.H. Bartholomew, Catalysis Reviews: Science and Engineering 24 (1982) 67–112.
[14] D.L. Trimm, Catalysis Reviews: Science and Engineering 16 (1977) 155–189.
[15] R.T.K. Baker, M.A. Barber, P.S. Harris, F.S. Feates, R.J. Waite, Journal of Catalysis 26 (1972) 51–62.
[16] J.R. Rostrup-Nielsen, D.L. Trimm, Journal of Catalysis 48 (1977) 155–165.
[17] R.T.K. Baker, Carbon 27 (1989) 315–323.
[18] S. Helveg, C. Lòpez-Cartes, J. Sehested, P.L. Hansen, B.S. Clausen, J.R. Rostrup-Nielsen, F. Abild-Pedersen, J.K. Nørskov, Nature 427 (2004) 426–429.
[19] S. Hofmann, R. Sharma, C. Ducati, G. Du, C. Mattevi, C. Cepek, M. Cantoro, S. Pisana, A. Parvez, F. Cervantes-Sodi, A.C. Ferrari, R. Dunin-Borkowski, S. Lizzit, L. Petaccia, A. Goldoni, J. Robertson, Nano Letters 7 (2007) 602–608.
[20] H.S. Bengaard, J.K. Nørskov, J. Sehested, B.S. Clausen, L.P. Nielsen, A.M. Molenbroek, J.R. Rostrup-Nielsen, Journal of Catalysis 209 (2002) 365–384.
[21] F. Abild-Pedersen, J.K. Nørskov, J.R. Rostrup-Nielsen, J. Sehested, S. Helveg, Physical Review B 73 (2006) 115419.
[22] J. Juan-Juan, M.C. Roman-Martinez, M.J. Illan-Gomez, Applied Catalysis A: General 301 (2006) 9–15.
[23] V.R. Choudhary, B.S. Uphades, A.S. Mamman, Catalysis Letters 32 (1995) 387–390.
[24] M. García-Diéguez, I.S. Pieta, M.C. Herrera, M.A. Larrubia, L.J. Alemany, Journal of Catalysis 270 (2010) 136–145.
[25] J.G. Zhang, H. Wang, A.K. Dalai, Journal of Catalysis 249 (2007) 300–310.
[26] K. Zhang, G.D. Zhou, J. Li, T.X. Cheng, Catalysis Communications 10 (2009) 1816–1820.
[27] J.R. Rostrup-Nielsen, Journal of Catalysis 85 (1984) 31–43.
[28] C.J. Liu, J.Y. Ye, J.J. Jiang, Y.X. Pan, ChemCatChem 3 (2011) 529–541.
[29] A. Trovarelli, Catalysis Reviews: Science and Engineering 38 (1996) 439–520.
[30] K.C. Taylor, Catalysis Reviews: Science and Engineering 35 (1993) 457–481.
[31] Y. Lu, J.C. Chen, Y. Liu, Q.S. Xue, M.Y. He, Journal of Catalysis 254 (2008) 39–48.
[32] Q.S. Xue, L.D. Gao, Y. Lu, Catalysis Today 146 (2009) 103–109.
[33] S.B. Wang, G.Q.M. Lu, Applied Catalysis B: Environmental 19 (1998) 267–277.
[34] C. Morterra, V. Bolis, G. Magnacca, Journal of the Chemical Society, Faraday Transactions 92 (1996) 1991–1999.
[35] J.G. Chen, J. Ren, Catalysis Letters 29 (1994) 39–48.
[36] X.J. Zou, X.G. Wang, L. Li, K. Shen, X.G. Lu, W.Z. Ding, International Journal of Hydrogen Energy 35 (2010) 12191–12200.
[37] S. Damyanova, C.A. Perez, M. Schmal, J.M.C. Bueno, Applied Catalysis A: General 234 (2002) 271–282.
[38] A. Piras, A. Trovarelli, G. Dolcetti, Applied Catalysis B: Environmental 28 (1) (2000) L77–L81.
[39] M. Matsukata, T. Matsushita, K. Ueyama, Energy & Fuels 9 (1995) 822–828.
[40] M. Matsukata, T. Matsushita, K. Ueyama, Chemical Engineering Science 51 (1996) 2769–2774.
[41] R.Q. Yang, C. Xing, C.X. Lv, L. Shi, N. Tsubaki, Applied Catalysis A: General 385 (2010) 92–100.
[42] S. Takenaka, E. Kato, Y. Tomikubo, K. Otsuka, Journal of Catalysis 219 (2003) 176–185.
[43] S. Takenaka, K. Otsuka, Chemistry Letters (2001) 218.
[44] K. Nagaoka, K. Seshan, K. Aika, J.A. Lercher, Journal of Catalysis 197 (2001) 34–42.
[45] Y. Saito, T. Toshikawa, S. Bandow, M. Tomita, T. Hayashi, Physical Review B 48 (1993) 1907–1909.
[46] N.M. Rodriguez, Journal of Materials Research 8 (1993) 3233–3250.
[47] C. Xie, Y.S. Chen, Y. Li, X.X. Wang, C.S. Song, Applied Catalysis A: General 394 (2011) 32–40.
[48] A.N.J. van Keulen, K. Seshan, J.H.B.J. Hoebink, J.R.H. Ross, Journal of Catalysis 166 (1997) 306–314.
[49] S.M. Staag, E.P. Salazar, C. Padro, D.E. Resasco, Journal of Catalysis 178 (1998) 137–145.
[50] S. Natesakhawat, R.B. Watson, X.Q. Wang, U.S. Ozkan, Journal of Catalysis 234 (2005) 496–508.
[51] J.W. Snoeck, G.F. Forment, M. Fowlest, Journal of Catalysis 169 (1997) 240–249.
[52] J.H. Bitter, K. Seshan, J.A. Lercher, Journal of Catalysis 183 (1999) 336–343.
[53] F. Abild-Pedersen, O. Lytken, J. Engbæk, G. Nielsen, I. Chorkendorff, J.K. Nørskov, Surface Science 590 (2005) 127–137.